Ammonium CI-Orbitrap: a tool for characterizing the reactivity of oxygenated organic molecules

Dandan Li[1], Dongyu Wang[2], Lucia Caudillo[3], Wiebke Scholz[4], Mingyi Wang[5,6], Sophie Tomaz[1], Guillaume Marie[3], Mihnea Surdu[2], Elias Eccli[4], Xianda Gong[7], Loic Gonzalez-Carracedo[8], Manuel Granzin[3], Joschka Pfeifer[3,9], Birte Rörup[10], Benjamin Schulze[6], Pekka Rantala[10], Sébastien Perrier[1], Armin Hansel[4], Joachim Curtius[3], Jasper Kirkby[3,9], Neil M. Donahue[5], Christian George[1], Imad El-Haddad[2], Matthieu Riva[1,*]

[1] Univ Lyon, Université Claude Bernard Lyon 1, CNRS, IRCELYON, 69626, Villeurbanne, France

[6] Institute for Atmospheric and Earth System Research/Physics, Faculty of Science, University of Helsinki, 00014, Helsinki, Finland

[2] Laboratory of Atmospheric Chemistry, Paul Scherrer Institute, 5232, Villigen, Switzerland

[3] Institute for Atmospheric and Environmental Sciences, Goethe University Frankfurt, 60438, Frankfurt am Main, Germany

[4] Institute for Ion Physics and Applied Physics, University of Innsbruck, 6020, Innsbruck, Austria

[5] Center for Atmospheric Particle Studies, Carnegie Mellon University, Pittsburgh, PA, 15213, USA

[6] now at Division of Chemistry and Chemical Engineering, California Institute of Technology, Pasadena, CA 91125, USA

[7] Leibniz Institute for Tropospheric Research, 04318, Leipzig, Germany

[8] Faculty of Physics, University of Vienna, Vienna, 1090, Austria

[9] CERN, the European Organization for Nuclear Research, CH-1211 Geneve 23, Switzerland

[10] Institute for Atmospheric and Earth System Research/Physics, Faculty of Science, University of Helsinki, 00014, Helsinki, Finland

[*] Email: matthieu.riva@ircelyon.univ-lyon1.fr

Abstract

Oxygenated organic molecules (OOMs) play an important role in the formation of atmospheric aerosols. Due to various analytical challenges in measuring organic vapors, uncertainties remain in the formation and fate of OOMs. The chemical ionization Orbitrap mass spectrometer (CI-Orbitrap) has recently been shown to be a powerful technique able to accurately identify gaseous organic compounds due to its great mass resolving power. Here we present the ammonium ion (NH_4^+) based CI-Orbitrap as a technique capable of measuring a wide range of gaseous OOMs. The performance of the NH_4^+-Orbitrap was compared with that of state-of-the-art mass spectrometers, including a nitrate ion (NO_3^-) based CI coupled to an atmospheric pressure interfaced to long time-of-flight mass spectrometer (APi-LTOF), a new generation of proton transfer reaction-TOF mass spectrometer (PTR3-TOF), and an iodide (I^-) based CI-TOF mass spectrometer equipped with a Filter Inlet for Gases and AEROsols (FIGAERO-CIMS). The instruments were deployed simultaneously in the Cosmic Leaving OUtdoors Droplets (CLOUD) chamber at the European Organization for Nuclear Research (CERN) during the CLOUD14 campaign in 2019. Products generated from α-pinene ozonolysis across multiple experimental conditions were simultaneously measured by the mass spectrometers. NH_4^+-Orbitrap was able to identify the widest range of OOMs (i.e., $O \geq 2$), from low oxidized species to highly oxygenated organic molecules (HOMs). Excellent agreements were found between the NH_4^+-Orbitrap and the NO_3^--LTOF for characterizing HOMs and with the PTR3-TOF for the less oxidized monomeric species. OOMs concentrations measured by NH_4^+-Orbitrap were estimated using calibration factors derived from the OOMs with high timeseries correlations during the side-by-side measurements. As other mass spectrometry techniques used during this campaign, the detection sensitivity of NH_4^+-Orbitrap to OOMs is greatly affected by relative humidity, which may be related to changes in ionization efficiency and/or multiphase chemistry. Overall, this study shows that NH_4^+ ion-based chemistry associated with the high mass resolving power of the Orbitrap mass analyzer can measure almost all-inclusive compounds. As a result, it is now possible to cover the entire range of compounds, which can lead to a better understanding of the oxidation processes.

1 Introduction

Aerosols affect the climate by either directly scattering or absorbing solar radiation, or acting as seeds for cloud formation (Fan et al., 2016; Haywood and Boucher, 2000). A major fraction of submicron aerosol mass consists of organic compounds, with secondary organic aerosol (SOA) predominating (Jimenez et al., 2009; Hallquist et al., 2009). Oxygenated organic molecules (OOMs) generated from the oxidation of volatile organic compounds (VOCs) contribute to the formation and growth of SOA (Ehn et al., 2014; Mellouki et al., 2015). OOMs can be generated through bimolecular peroxy radicals (RO_2) pathway or by the autoxidation of RO_2 followed by the termination pathways (Bianchi et al., 2019; Mohr et al., 2019). Among the OOMs, the highly oxygenated organic molecules (HOMs), containing multiple functional groups and exhibiting (extremely) low saturation vapor pressure, can nucleate in concert with inorganic species e.g., sulfuric acid or on their own (Ehn et al., 2014; Kirkby et al., 2016; Bianchi et al., 2016), forming new particles. Less oxygenated molecules (i.e., containing 2 to 5 oxygen atoms) play a vital role in the growth of newly formed atmospheric particles, either by condensation or through multiphase chemistry (Bianchi et al., 2019; Ehn et al., 2014; Hallquist et al., 2009). Therefore, the identification and quantification of the wide diversity of OOMs are essential to understand SOA formation and growth (Kirkby et al., 2016; Bianchi et al., 2016; Ehn et al., 2014).

Mass spectrometry (MS) has made remarkable achievements in detecting, characterizing, and quantifying OOMs (Wang et al., 2020; Breitenlechner et al., 2017; Bianchi et al., 2019; Ehn et al., 2010; Riva et al., 2019a). Moreover, the application of chemical ionization (CI) enables the detection of a wide variety of organic and inorganic analytes (Bianchi et al., 2019; Ehn et al., 2014; Jokinen et al., 2012; Lee et al., 2014). However, the selection of ionization chemistry in combination with MS detection technique will impact the methods selectivity and sensitivity toward certain groups of OOMs (Bianchi et al., 2019; Riva et al., 2020; Riva et al., 2019b; Berndt et al., 2018b; Berndt et al., 2018a). For example, negative ion-based chemistry, including nitrate (NO_3^-), can optimally detect HOMs, which only constitute a small subset of the OOMs (Lee et al., 2014; Berndt et al., 2018b; Riva et al., 2019b); iodide (I^-) can efficiently detect various OOMs with 3-5 oxygen atoms (Riva et al., 2019b; Lee et al., 2014). Positive ion-based chemistries have also been developed, showing great sensitivity to HOMs as well as less oxidized products, providing the possibility of achieving carbon closure of the OOMs (Berndt et al., 2018a; Berndt et al., 2018b; Hansel et al., 2018; Riva et al., 2020; Riva et al., 2019b). However, these positive ion methods are mainly based on proton transfer and often result in fragmentation of the analytes (Breitenlechner et al., 2017). Time-of-flight (TOF) mass spectrometers using ammonium (NH_4^+) or amines as reagent ions can detect a wide variety of OOMs but suffer from a lack of mass resolving power, making peak identification challenging, especially for complex systems, i.e., under ambient conditions (Berndt et al., 2018b; Berndt et al., 2018a; Riva et al., 2019b). Finally, the recently developed Orbitrap mass spectrometer using propylamine has achieved unambiguous identification of overlapping peaks and accurate quantification of OOMs (Riva et al., 2020). However, this analytical technique has been used in very diluted and dry environments to ensure a linear response to the OOMs produced from simple atmospheric systems, i.e., a single VOC precursor and oxidant (Riva et al., 2020; Riva et al., 2019b).

Here, we explore the capability of NH_4^+ ion-based CI-Orbitrap mass spectrometer (Q-Exactive Orbitrap, Thermo Scientific) for detecting OOMs generated from α-pinene ozonolysis in the Cosmic Leaving OUtdoors Droplets (CLOUD) chamber at the European Organization for Nuclear Research (CERN) under various environmental conditions. We compare the performance of the NH_4^+-Orbitrap to state-of-the-art online mass spectrometers including a nitrate CI atmospheric pressure interface long time of flight mass spectrometer (NO_3^--LTOF; Tofwerk AG), a proton transfer reaction time of flight mass spectrometer (PTR3-TOF; Ionicon Analytik GmbH), and gas phase of an iodide CI time of flight mass spectrometer equipped with a Filter Inlet for Gases and AEROsols (I^--CIMS, Tofwerk AG).

2 Experimental approach and product analysis

2.1 CLOUD chamber experiments

All experiments were conducted in the CLOUD chamber, a 26 m^3 cylindrical stainless-steel vessel at CERN. The chamber can achieve a pristine background for the study of nucleation (Kirkby et al., 2016). The chamber operated as a continuously stirred tank reactor (CSTR), with mixing driven by two inductively coupled fans at the top and bottom of the chamber. Evaporated liquid nitrogen (N_2) and liquid oxygen (O_2) were blended at a ratio of 79:21 to provide ultra-pure synthetic air, which flushed the chamber constantly. Variable amounts of trace gases, including O_3, VOCs, NO_x, SO_2, and CO were accurately injected into the chamber via a gas control system and monitored. Photolysis was driven by various light sources, including Hg-Xe UV lamps, and UV excimer laser. Between experiments, the chamber was cleaned by irrigating the walls with ultra-pure water, then heated to 373 K, and flushed with humidified pure air and high ozone, reducing the contaminant (e.g., VOCs) to sub pptv levels. During the cleaning process, particles were removed using a high-voltage electric field.

The results presented here were from the CLOUD14 campaign performed in autumn 2019. During CLOUD14, the total flow was kept at 250 standard liters per minute (slpm), providing an average residence time of 104 minutes. α-Pinene was introduced into the chamber by passing a small flow of dry air over a temperature-controlled evaporator containing liquid α-pinene. Ozone was generated by flowing a small fraction of the air through a quartz tube surrounded by UVC lights (wavelength < 240 nm). Experiments were performed at low temperature (263 ± 0.1 K). The RH in the chamber was controlled by flowing a portion of the air through a Nafion® humidifier using ultrapure water (18 MΩ cm, Millipore Corporation). The contents of the chamber were monitored by a wide range of external instruments connected to the sampling probes that protrude ~1 m into the chamber.

2.2 Product analysis by NH_4^+-Orbitrap

The chemical composition of closed-shell molecules was determined in real time by means of a CI-Orbitrap sampling from the CLOUD chamber through a 750 mm long, 10 mm inner diameter Teflon tube at a flow rate of 10 slpm. The CI inlet mounted on the Orbitrap was custom-built with minor modifications from the commercial inlet (Riva et al., 2019a). The ion-molecule reaction (IMR) proceeded at atmospheric pressure with a residence time of 200-300 ms. The same operating parameters used in our previous studies (RF level 60, automatic gain control 1×10^6 charges, maximum injection time 1000 ms, multi RF ratio 1.2, mass resolution m/Δm 140,000 at *m/z* 200), were used, thereby minimizing declustering and maximizing the linearity range (Riva et al., 2019a; Riva et al., 2020; Cai et al., 2022).

The high resolution Orbitrap mass spectra data were analyzed using "Orbitool" software with a graphical user interface (GUI) (https://orbitrap.catalyse.cnrs.fr) (Cai et al., 2021). The analysis procedures included data averaging, noise determination and reduction, single peak fitting, mass calibration, assignment of molecular formulas, and export of time series. Signals were averaged over 5 min before determining the noise and performing mass calibration.

NH_4^+ has been utilized in PTR-MS with a low pressure (Berndt et al., 2018b; Hansel et al., 2018). Here, this ionization technique was used to detect OOMs in atmospheric pressure and was operated in a similar fashion as in our initial study (Riva et al., 2019a). NH_3 was added into the ion source by flushing 2 sccm of dry air over the headspace of a 1% liquid ammonia water mixture (prepared from a MilliQ water and a 25% ammonium hydroxide stock solution, ACS reagent, Sigma-Aldrich). The product molecules ("prod") were softly charged by binding to ammonium (NH_4^+) ions, forming (prod)-NH_4^+ adduct ions or protonated products (prod)-H^+, following either reaction (1) or (2),

$$NH_4^+ + \text{prod} \rightarrow (\text{prod})\text{-}NH_4^+ \quad (1)$$

$$NH_4^+ + \text{prod} \rightarrow (\text{prod-H})^+ + NH_3 \quad (2)$$

The NH_4^+ reagent ion cannot be directly detected due to the cut-off of the Orbitrap mass analyzer (i.e, m/Q 50). Hence, normalization of the raw analyte signals is difficult and hinders quantification of OOMs. However, we observed a total of 62 peaks corresponding to amines, including $C_4H_{12}N^+$, and $C_6H_{14}N^+$, which are formally ammonia derivatives. To some extent, their signals can be used to correct for changes in NH_4^+ ion chemistry. Among these peaks, 13 were abundant and constant throughout the measurement period (Fig. S1). As a result, these signals were used as surrogates for the primary reagent ions to normalize the signal intensity of the OOMs (equation 3) and to account for the potential variation of the ionization process (Riva et al., 2019b).

$$[OOM]_{nor} = \frac{[(OOM)-NH_4^+] + [(OOM-H)^+]}{\sum[Amine]} \quad (3)$$

Correlation analysis were performed between the NH_4^+-Orbitrap and the two reference instruments including NO_3^--LTOF and PTR3-TOF (referred to as REF). The Pearson correlation coefficients (R^2) were determined using the timeseries during two runs (run 2211 and 2213). This included AP injection, steady state stage, NO_x or CO injections, and RH variation. As a result, for one compound, 755 data points were recorded and used for the correlation analysis. Although product ions with same molecular formulas might lead to low correlation (See details in section 3.3) and would suggest different species (i.e., isomers, fragment ions,…), a few molecules with R^2 greater than 0.9 (18 for NO_3^--LTOF, 32 for PTR-TOF, and 5 for I^--CIMS) were selected and be likely attributed to the same species.

Although no direct calibration has been performed for the NH_4^+-Orbitrap, the OOM concentrations were estimated based on comparisons between NH_4^+-Orbitrap and the two reference instruments which has developed reliable quantification methods. For the OOMs whose timeseries had R^2 greater than 0.9 between NH_4^+-Orbitrap and REF, linear regression was conducted for normalized intensities in NH_4^+-Orbitrap (dimensionless) and concentrations in REF (molecules cm^{-3}), and the slopes were recorded as their relative sensitivity. The calibration factor $\mathrm{c_{Orbi-REF}}$ was derived from the averaged relative sensitivity of these species (~2.62×10^8 molecules cm^{-3} for NO_3^--LTOF and ~4.83×10^8 molecules cm^{-3} for PTR3-TOF). Applying the calibration factors to all the OOMs, their concentrations detected by NH_4^+-Orbitrap could be calculated as shown in equation (4). Additionally, a temperature-dependent sampling-line loss correction factor was applied (Simon et al., 2020).

$$[OOM]_{Orbi-REF} = c_{Orbi-REF} \times [\mathrm{OOM}]_{nor} \tag{4}$$

2.3 Product analysis by NO_3^--LTOF

Detection of RO_2 radicals and closed-shell products was also performed by the NO_3^--LTOF which has been described elsewhere (Jokinen et al., 2012; Caudillo et al., 2021). Therefore, only relevant details for this study are provided here. The NO_3^--LTOF used in this study had a mass resolving power of m/Δm 12,000 and detected OOMs (mass 300-650 Da) as clusters ions with $(HNO_3)_n(NO_3^-)$ anions, with n = 0-2. The limit of detection (LoD) for OOMs is 5×10^4 molecules cm^{-3} (Simon et al., 2020). The primary ions were produced by a corona discharge needle exposed to a sheath gas enriched by HNO_3. Laminar flow diffusional loss was assumed in the 30 cm sampling line. A core-sampling technique was applied , which drew a core flow of 5.1 slpm from the center of a 30 slpm total flow. This setup reduced the sampling loss rate of HOMs to less than 30% (Simon et al., 2020).

The data were processed using Tofware (Version 3.2, Aerodyne Inc., USA) and MATLAB R2019b (MathWorks, Inc., USA). In addition, background signals, mass-dependent transmission efficiency (Heinritzi et al., 2016), and sampling losses (Simon et al., 2020) were determined and corrections were applied. The NO_3^--LTOF was directly calibrated using sulfuric acid (H_2SO_4), where the detection efficiency of HOMs was assumed as similar to H_2SO_4 . However, OOMs with less oxygen number (O < 6) were prone to a lower detection efficiency compared to H_2SO_4, leading to an underestimation (Stolzenburg et al., 2018; Ehn et al., 2014). A calibration factor C was determined to be ~4.13×10^{10} molecules cm^{-3} during CLOUD14 (Caudillo et al., 2021). The concentration of OOMs was also corrected using a mass dependent transmission efficiency inferred by depleting the reagent ions with several perfluorinated acids. Assuming that OOMs got lost in sampling lines due to diffusion, the losses of OOMs were corrected with a diffusion coefficient scaling with the molecular mass. More information could be found in former studies (Heinritzi et al., 2016; Stolzenburg et al., 2018; Simon et al., 2020; Caudillo et al., 2021).

2.4 Product analysis by PTR3-TOF

The PTR3-TOF ionizes organic compounds by proton transfer or ligand swith reactions where protonated water clusters $(H_2O)_nH_3O^+$ with n=1-3 were produced by a corona discharge using humidified nitrogen (Breitenlechner et al., 2017). To reduce sample losses, a 2 slpm was drawn from a 10 slpm laminar flow through a critical orifice into the tripole where the ion-molecule reactions occur. The pressure in this region was maintained at ~80 mbar. The distribution of primary ions and sample molecules can be adjusted by a tunable radio frequency signal applied to the tripole rods. The LoD of PTR3-TOF for detecting OOMs is 8×10^5 molecules cm^{-3} (Breitenlechner et al., 2017).

During the CLOUD14 experiments, the collision energy was controlled between 62 and 72 Td to reduce the methods humidity dependence which may complicate the detection of organic compounds. A gas standard mixture containing 1 ppm of 3-hexanone, heptanone, and α-pinene in nitrogen was dynamically diluted by a factor of 1000 in VOC-free air to contain 1 ppbv of each compound, and then was used to calibrate the PTR3-TOF. All data were analyzed using TOF-Tracer software running on Julia 0.6 (https://github.com/lukasfischer83/TOF-Tracer) and were further corrected for the duty cycle transmission of TOF and temperature dependent sampling line losses (Stolzenburg et al., 2018). On the one hand, duty cycle corrected counts per second dcps, $dcps_i = cps_i \times (101/m_i)^{1/2}$, was utilized to account for the mass-dependent transmission of the TOF mass spectrometer (Breitenlechner et al., 2017). The calculated sensitivities of 3-hexanone and heptanone were comparable to the observed ones. Therefore, the concentration of oxygenated products was estimated using the sensitivity of 3-hexanone as lower-limit values due to possible fragmentation (Breitenlechner et al., 2017; Stolzenburg et al., 2018). On the other hand, the detected OOMs having (extremely) low volatility were assumed to be lost by diffusion and adjusted by a temperature dependent loss-correction. The sampling line losses considered three loss sections under different temperatures, including losses at the sampling lines within and outside the chamber and within the PTR3-TOF instrument. Details can be found in previous studies (Breitenlechner et al., 2017; Stolzenburg et al., 2018).

2.5 Product analysis by I^--CIMS

The I^--CIMS was capable of characterizing both gas and particle phases (Lopez-Hilfiker et al., 2014). In the gas-phase mode, gases were directly sampled into a 100-mbar turbulent ion-molecule reactor, while particles were collected onto a polytetrafluoroethylene (PTFE) filter through a separate dedicated sampling port. Analytes were then ionized with I^- chemical ionization and extracted into a TOF mass analyzer (Wang et al., 2020). The LoD of I^--CIMS for OOMs could be lower to ~10^7 molecules cm^{-3} (Lee et al., 2014). In this study, only gas phase data are reported.

Iodide ions (I^-) were used as the reagent ions and formed by passing a 1.0 slpm flow of ultrahigh purity N_2 over a diffusion tube filled with methyl iodide (CH_3I), and then through a ^{210}Po radioactive source. In the sampling mode, the reagent ion flow was mixed with a sample flow in the IMR at ~150 mbar. Coaxial core sampling was used to minimize the vapor wall loss in the sampling line. The total flow was kept at 18.0 slpm and the core flow at 4.5 slpm; the instrument sampled at the center of the core flow with a flow rate of 1.6 slpm. The gas-phase background signal was determined by routinely introducing zero air directly into the inlet. Data were analyzed using Tofware (2.5.11_FIGAERO version; Aerodyne Inc., USA) giving 10 s average mass spectra. The ion signal was normalized by the sum of reagent ion signals (i.e., m/Q 127: I^- and 145: H_2OI^-).

2.6 Volatility of OOMs

It is challenging to directly measure the vapor pressure of individual OOMs due to the difficulty to acquire authentic standards. To overcome experimental challenges, model calculations have been developed to estimate the vapor pressure using, for example, structure-based estimations and formula-based estimations (Pankow and Asher, 2008). Volatility basis set (VBS), a categorization framework based on quantifiable organic property (i.e., volatility) has been established and is frequently used to characterize oxidation chemistry (Donahue et al., 2011; Li et al., 2016). The VBS parameterization is useful for classifying the wide range of OOMs into multiple volatility groups, including extremely low volatility organic compounds (ELVOC) and low volatility organic compounds (LVOC) based on their effective saturation concentration (C^*) in the unit of μg m^{-3} (Bianchi et al., 2019). In this study, we applied the VBS parameterization optimized by Li et al (Li et al., 2016; Isaacman-Vanwertz and Aumont, 2021).

$$log_{10}C^*(298K) = \left(n_C^0 - n_C\right)b_C - n_O b_O - 2\frac{n_C n_O}{(n_C+n_O)}b_{CO} - n_N b_N - n_S b_S \quad (5)$$

where n_C, n_O, n_N, and n_S was the number of carbon, oxygen, nitrogen, and sulfur atoms of the specific molecule, separately; n_C^0 was the reference carbon number; b_C, b_O, b_N, and b_S was the contribution of each atom to $log_{10}C^*$, respectively; b_{CO} was the carbon-oxygen nonideality (Donahue et al., 2011). Values of b coefficient can be found in Li et al.(Li et al., 2016). The formula used to estimate the vapor pressure was amended to convert all NO_3 groups into OH groups to reduce the bias from the compounds containing nitrates (Daumit et al., 2013; Isaacman-Vanwertz and Aumont, 2021).

Due to the different temperatures in the CLOUD14 experiments, we adjusted $C^*(298K)$ to the measured experimental temperature in equations (6) and (7):

$$log_{10}C^*(T) = log_{10}C^*(298K) + \frac{\Delta H_{vap}}{Rln(10)} \times \left(\frac{1}{298} - \frac{1}{T}\right) \quad (6)$$

$$\Delta H_{vap}(kJ\ mol^{-1}) = -11 \cdot log_{10}C^*(298K) + 129 \quad (7)$$

where T was the temperature in Kelvin, $C^*(298K)$ was the saturation vapor concentration at 298 K, ΔH_{vap} was the evaporation enthalpy and R was the gas constant (8.3134 J K^{-1} mol^{-1}). The potential presence of isomers may result in uncertainty in this method since the only input is the compound's molecular formula.

In this study, all oxidation products were grouped into six volatility regimes; ultralow-volatility (ULVOCs, $C^* < 10^{-8.5}$ μg m^{-3}), extremely low volatility (ELVOCs, $10^{-8.5} < C^* < 10^{-4.5}$ μg m^{-3}), low-volatility (LVOCs, $10^{-4.5} < C^* < 10^{-0.5}$ μg m^{-3}), semi-volatile (SVOCs, $10^{-0.5} < C^* < 10^{2.5}$ μg m^{-3}), intermediate-volatility organic compounds (IVOC, $10^{2.5} < C^* < 10^{6.5}$ μg m^{-3}), and VOC ($10^{6.5} < C^*$ μg m^{-3}) based on VBS.

3 Results and Discussions

3.1 Peak identification of NH_4^+-Orbitrap

As a promising reagent ion for detecting the full range of OOMs, more ions with low concentration were captured by NH_4^+, whose identification and quantification were most affected by overlapping signals. The relative intensities of neighboring peaks should also be considered when estimating their ease of separation. It has been shown that the higher mass resolution reduced the interference of adjacent peaks based on NO_3^- or $C_2H_3O_2^-$ reagent ions (Riva et al., 2019a; Riva et al., 2020). Therefore, the ability of the NH_4^+-Orbitrap for separating overlapping mass spectral peaks was compared to NH_4^+-TOF.

The mass resolving power was defined as the ratio of m to Δm, where m was the mass-to-charge ratio of the analyte ion, and Δm was the full width at half maximum (FWHM). Higher mass resolving power allows unambiguous mass spectral peak assignment. For a pair of overlapping peaks of equal intensity, the distance between their respective peak center, referred to hereafter simply as peak distance, *dm*, needed to be greater than approximately 0.8 of the FWHM of the overlapping peaks, such that they could be reasonably deconvolved as shown in Fig. S2. Depending on their experience, individuals may be able to visually identify the presence of overlapping peaks at lower or higher *dm* values. We arbitrarily defined the minimum *dm* (normalized to that of FWHM, or Δm) as the value at which the observed spectrum ("Combined" trace in Fig. S2 and S3) had a local minimum between the centers of the overlapping peaks (i.e., there was a "dip" in the observed signal between ion peaks). The minimum *dm* value increased with the intensity ratio of overlapping peaks, ranging roughly from 0.85 (for equally intense peaks) to 1.43 (for peaks differing one order of magnitude in their respective intensities), as shown in Fig. S3. In practice, noise and the presence of additional neighboring peaks would further complicate peak deconvolution. For simplicity, we used a normalized *dm* of 1 (i.e., $dm = \Delta m$) as a threshold for unambiguous deconvolution of neighboring peaks.

Figure 1 shows the histogram of the distances between neighboring peaks normalized against the FWHM for the NH_4^+-Orbitrap and the NH_4^+-TOF having a mass resolving power of 10,000. In each histogram, one count indicated that an ion had at least one neighboring ion with a relative intensity of 20%, 50%, or 100% (with a higher relative intensity threshold value being less selective). Neighboring ions separated by distances exceeding 2 times the FWHM were considered well-separated. For ions with multiple neighboring peaks within the 2 x FWHM separation distance window, the distance to the first neighboring peak that satisfied the aforementioned relative intensity threshold was reported. Overall, NH_4^+-Orbitrap can separate most of the observed ions (> 99%), while the NH_4^+-TOF, depending on the relative intensity threshold set, can separate only 32% to 46% of all the ions by at least 1 FWHM. It should be noted that the NH_4^+-Orbitrap has shown its strength in separating neighboring peaks in controlled experiments, in which the knowledge of the chemical compositions for OOMs is relatively abundant. The advantages of higher mass resolving power should be further stressed in ambient observations, where the knowledge about OOM species can be limited with a larger number of detectable peaks.

3.2 Characterization of OOMs by four instruments

llustrated in Fig. 2 are mass defect plots of OOMs measured by NH_4^+-Orbitrap, NO_3^--LTOF, PTR3-TOF, and I^--CIMS, identifying species of 484, 252, 145, and 67, respectively in run 2211. The NH_4^+-Orbitrap detected the widest range of products, including HOMs and the less oxidized species (i.e., O < 6). Out of the 484 compounds, 5% were amines. The number of O atoms in OOMs varied from 1 to 11 in monomers ($C_{2\text{-}10}$) and from 2 to 16 for dimeric products ($C_{14\text{-}20}$), with an average elemental oxygen-to-carbon ratio (O:C) of 0.4 ± 0.2 (the value following "±" herein and after refers to the standard deviation of O:C during the experiment). As expected, the NO_3^--LTOF exhibited a very good sensitivity towards HOMs, with the highest O:C of 0.7 ± 0.3. The PTR3-TOF mainly detected compounds below m/Q 300 Th with an average O:C of 0.5 ± 0.3, which was due to the optimization to (i.e., lowering E/N value) measure ammonia and amines sensitively, which ultimately impacted its capability to detect efficiently OOMs. However, many less oxygenated OOMs were still observed by the PTR3-TOF and were used to conduct the correlation analysis of time series with those detected by the NH_4^+-Orbitrap. Due to the selectivity and potential losses within the sampling line/inlet of the I^--CIMS equipped with a FIGAERO inlet fewer monomers of $C_{8\text{-}10}$ and dimers of $C_{19\text{-}20}$ were observed, with an average O:C of 0.5 ± 0.2.

3.3 Instrumental comparisons: correlations

Due to differences in selectivity and sensitivity of the analytical methods toward OOMs, ~42% of the identified species by NH_4^+-Orbitrap are simultaneously detected by other mass spectrometers (Fig. S4). To identify how NH_4^+-Orbitrap performed compared to the other mass spectrometers, a correlation analysis including all co-detected ions was complied. The experimental conditions of the runs used for performing this analysis are summarized in Table S1. The data set covered a variety of conditions, such as different concentrations of α-pinene, NO_x, SO_2, and CO, as well as RH. R^2 was calculated, using the time series of OOMs having the same elemental composition measured by the different mass spectrometers. Figure 3 displays the correlation coefficient of time series for the detected compounds, with marker size scaled by R^2. The NH_4^+-Orbitrap and the NO_3^--LTOF detected OOMs with the same chemical compositions, covering monomers and dimers, among which 18 OOMs showed $R^2 > 0.9$. Regarding the PTR3-TOF, the NH_4^+-Orbitrap demonstrated high correlations for most of the monomers and fewer dimers, including 32 species having an $R^2 > 0.9$. Due to potential losses within the FIGAERO inlet, fewer OOMs were detected by the I^--CIMS. However, certain families of compounds, including $C_{10}H_{15}O_{5\text{-}7}N$ and $C_{20}H_{31}O_{7,9}N$ showed high correlations (i.e., $R^2 > 0.9$) between the NH_4^+-Orbitrap and with the I^--CIMS. Finally, the NO_3^--LTOF was regarded as the reference instrument for HOMs measurements. Only fewer monomers with high oxygen content were detected by the NO_3^--LTOF and the PTR3-TOF, and only a few dimers between the NO_3^--LTOF and the I^--CIMS with moderate relevance.

The reason why the correlations of certain molecules are lower than 0.9 might be due to the molecules' composition or potential ionization artifacts. RH dependence is an important property leading to the low correlations as the experiment includes RH variation from 20% to 80%. Although

NO_3^- ion chemistry had been reported to be less dependent on RH (Viggiano et al., 1997), the sensitivities of PTR3-TOF (Breitenlechner et al., 2017) and I^--CIMS (Lee et al., 2014) both showed high dependence on RH. In addition, the relative sensitivity of NH_4^+-Orbitrap was also influenced by the varying RH (See details in Section 3.6). Fragmentation, such as decomposition of dimers, would also lead to low correlations. However, less fragmentation is expected to occur in the NH_4^+-Orbitrap using similar settings as our earlier studies (Riva et al., 2019a; Riva et al., 2020). In comparison, decomposition of peroxides (i.e., ROOR and ROOH) can be expected within the PTR3-TOF. While fragmentation of dimeric compounds can contribute to the overall signal of the monomers, the concentration of such species remains minor (Li et al., 2022). As a result, no large enhancement of the monomers signal intensity is expected. There are also other artifacts which cannot be excluded based on current dataset, including potential isomers and differences in response time between instruments, would also lead to the low correlations. However, by comparing the coverage regions of the instruments across multiple experimental conditions, the NH_4^+-Orbitrap was capable of covering the widest range of compounds and showed an overall good agreement with other mass spectrometers.

3.4 Instrumental comparisons: concentration estimates

Concentrations of the identified compounds were estimated for NH_4^+-Orbitrap, as described in section 2.2. The sensitivity of NH_4^+-Orbitrap was constrained based on the intensity comparison between NH_4^+-Orbitrap and the other two instruments. For instance, concentrations of the most abundant C_{10}-monomers (i.e., $C_{10}H_{14/16}O_n$) were estimated using different calibration factors (Fig. 4), which were measured during steady-state conditions (i.e., Run 2211 with $[O_3]$ = 100 ppbv and [α-pinene] = 2 ppbv, RH = 10%). The concentrations of C_{10}-monomers measured by the NH_4^+-Orbitrap based on the two calibration factors vary within a factor of 2, which indicates the consistency between the two correlation analyses. The variation trend of concentrations with the oxygen number of the NH_4^+-Orbitrap is similar to that of the NO_3^--LTOF in the range of $n_O>6$, and it is similar to that of the PTR3-TOF in the range of $n_O=1\sim5$. Taking into consideration that such ranges are also the oxygen number ranges with high sensitivities respectively, this proves the robustness of the NH_4^+-Orbitrap and the intensity-based relative comparison between NH_4^+-Orbitrap and two reference instruments. As previously reported, the Orbitrap had a non-linear response to compounds present at extremely low concentrations, which was independent of the sample composition, instrumental setup, or the reagent ion (Riva et al., 2020; Cai et al., 2022). A similar evaluation was performed for the NH_4^+-Orbitrap by comparing the measured versus the theoretical isotopic intensities. As shown in Fig. S5, the NH_4^+-Orbitrap had a linear response for ion intensity greater than $\sim5 \times 10^3$ cps, which corresponded to a limit of quantification (LoQ, corresponding to the lowest normalized signal observed within the linear range) of $\sim5 \times 10^5$ molecules cm^{-3} for OOMs, estimated using the calibration factor derived from the NO_3^--LTOF; which is consistent with a previous study (Riva et al., 2020).

Figure 5 presents the concentrations of all OOMs measured by the NH_4^+-Orbitrap determined by applying two different calibration factors. The concentrations of OOMs measured by the NH_4^+-Orbitrap were higher than both the NO_3^--LTOF and the PTR3-TOF which was optimized for measuring ammonia and amines. This indicates that the NH_4^+-Orbitrap can provide a better constraint on the concentrations of the primary products. As an example, pinonaldehyde (i.e., $C_{10}H_{16}O_2$), as one of the most abundant oxidation products, was not efficiently detected by the NO_3^--LTOF, which is consistent with the higher selectivity of the NO_3^- reagent ion. To further illustrate the selectivity of the different reagent ions, Fig. 6 offers a summary of the performance of each mass spectrometer in detecting monomeric compounds, such as $C_{10}H_{16}O_n$. The y-axis is arbitrary and represents a qualitative characterization of the oxygen content when compounds were detected by different CI schemes. Similar to previous results, the I^--CIMS detected OOMs with $n_O > 3$, but was not optimal for the detection of monomers with $n_O > 7$ (Riva et al., 2019b). The NO_3^--LTOF was mainly selective towards HOMs with $n_O > 6$ (Riva et al., 2019b). The PTR3-TOF had limited capabilities in detecting OOMs with $n_O > 5$ due to the optimization of the instrument to obtain a very sensitive measurement of ammonia. Previously, the amine-CI demonstrated promise for the detection of OOMs, but was limited to applications with comparatively clean conditions due to considerable depletion of the reagent ion and the presence of overlapping peaks (Berndt et al., 2018b; Riva et al., 2019b). While showing a similar OOMs detection range to amine-CI, NH_4^+-CI in tandem with the greater mass resolving power of the Orbitrap mass analyzer provided a linear response to higher loading. As shown in Fig. S6, background peaks were not affected by atmospherically relevant concentrations of O_3 and α-pinene. Overall, the NH_4^+-Orbitrap appears to have the potential for providing a more reliable identification/quantification of OOMs produced from VOC oxidation compared to other existing mass spectrometry techniques.

3.5 Volatility distribution by four instruments

Figure 7 shows the distribution of oxidation products measured by four MS instruments according to their saturation vapor concentrations ($\log_{10}C_{\mathrm{sat}}$) estimated using the modified Li et al. approach (Li et al., 2016; Isaacman-Vanwertz and Aumont, 2021). OOMs were grouped into six volatility regimes based on a volatility basis set (VBS): ultra-low volatility (ULVOCs); extremely low volatility (ELVOCs); low-volatility (LVOCs); semi-volatile (SVOCs); intermediate volatility organic compounds (IVOC); and VOC. ULVOCs and ELVOCs initiate cluster growth and form new particles. The total signal in each volatility bin represented the sum of the signal intensity of OOMs within the volatility range. The mean contributions of these compound regimes are shown in the VBS pie charts. The ULVOC, ELVOC, and LVOC regimes were well captured by NH_4^+-Orbitrap and NO_3^--LTOF. The PTR3-TOF only characterized the SVOC and IVOC regime (along with VOCs). IVOC and VOC regimes in the PTR3-TOF and NH_4^+-Orbitrap were generally less oxygenated VOCs (i.e., $n_O < 5$). IVOC comprised the biggest mass contributions for the NH_4^+-Orbitrap, and LVOC dominated in the NO_3^--LTOF. Hence, the detection of the NH_4^+-Orbitrap covered the widest range of volatilities, clearly highlighting the benefit of using this technique for the formation and fate of OOMs. In the past, reagent switching has not been practical, and users would run multiple mass spectrometer systems in parallel or use a Multi-scheme chemical IONization inlet (MION) with only one mass spectrometer to obtain the fullest possible mass spectrum (Rissanen et al., 2019; Huang et al., 2021). With NH_4^+-Orbitrap it is now possible to cover the entire range of compounds which was not the case with most CI techniques.

3.6 RH dependance of NH_4^+-Orbitrap

The sensitivity of the reagent-adduct ionization has been reported to be affected by the presence of water vapor for a variety of reagent ions (Lee et al., 2014; Breitenlechner et al., 2017). The impact of RH on the detection of OOMs by the NH_4^+-Orbitrap was also studied. While the concentrations of gas phase precursor and oxidant remained constant, the RH was raised from 10% to 80%. During this increase the signal of organic vapor behaved inconsistently under an otherwise constant gas-phase production rate (Surdu et al., 2023) and an increase in the condensation sink (Fig. S7). As shown in Fig. 8, the NH_4^+-Orbitrap demonstrated an RH dependence. For instance, the signal of less oxygenated molecules (i.e., $n_O < 5$) increased with increasing RH, especially compounds with $n_C = 8$; while the signal of highly oxygenated molecules (i.e., $n_O > 10$) decreased as a function of RH. The average behavior of all C_{8-10} monomers and C_{18-20} dimers was summarized and compared between four instruments (Fig. S8). The other three mass spectrometers also showed obvious RH dependence. Similar to NH_4^+-Orbitrap, OOMs with $n_O < 5$ measured by NO_3^--LTOF and PTR3-TOF increased at high RH, and a reverse tendency for HOMs with $n_O > 11$, while OOMs with $n_O = 8\sim11$ seemed to be independent to RH. The large variations of OOMs intensity at different RH measured by NH_4^+-Orbitrap may be due to the widest range of oxygen atoms. The causes why OOMs with different oxygen numbers measured by four instruments changed with RH was not clear. Here, multiple possible reasons were provided to explain the signal evolution of the ions with changing RH, such as water affecting the ionization efficiency or altering the physicochemical processes of the gas phase chemistry.

First, the efficiency of a particular compound partly relied on whether water vapor competes with the ammonium ion, lowering the sensitivity, or whether it acted as a third body to stabilize the ammonium-organic analyte cluster by removing extra energy from the collision, raising the sensitivity (Lee et al., 2014). NH_4^+ primary ions can cluster with water molecules when humidity increased, thereby reducing the clustering of the NH_4^+ with organic analytes (Breitenlechner et al., 2017). However, the formed $NH_4^+X_n$ (X being NH_3 or H_2O; n = 1,2) clusters might also act as reagent ions and ionize OOMs through ligand switching reactions, which were expected to be fast and thus improve the charging efficiency (Hansel et al., 2018). Compared to previous NH_4^+-CIMS, the $NH_4^+X_n$ reagent ions were expected to be larger due to the absence of the field in the ion-molecular-reaction zone in Orbitrap, resulting in greater ligand exchanging and increasing the sensitivity for the less oxygenated species (Canaval et al., 2019).

For RH-independent compounds, this may be due to the existence of very stable complexes with NH_4^+ reagent ion, or sufficient internal vibrational modes to disperse extra energy from the collision (Lee et al., 2014). The highly oxygenated dimers in the category of ULVOCs and ELVOCs which largely partition to the particle phase regardless of the presence of water might indicate that water may also affect the physicochemical processes (i.e., multiphase chemistry, partitioning, etc.), in this case possibly leading to an increase in the driving force of gas-particle partitioning of highly oxygenated species (Surdu et al., 2023), and/or causing the decomposition of highly oxygenated molecules in the particle phase to create less and moderately oxygenated products, e.g., $C_8H_{12}O_{1-5}$ (up to a 30-fold increase in the gas phase) (Pospisilova et al., 2020), although which in the range of SVOCs (e.g., $C_8H_{12}O_{4,5}$) was also thought to partition more to the particle phase at higher RH (Surdu et al., 2023). Finally, while water vapor could affect the gas-phase chemistry through water reactions with the Criegee intermediates (CIs), HO_2 chemistry, OH radical concentration, no clear evidence has been identified as earlier discussed by Surdu et al (2023). However, the accurate reasons needs to be further verified in target control experiments like changing the RH in IMR of CI inlet.

4 Summary

In conclusion, this study presented an intercomparison between NH_4^+-Orbitrap, NO_3^--LTOF, PTR3-TOF, and I^--CIMS based on the identification and quantification of OOMs formed from the ozonolysis of α-pinene under various environmental conditions. We used NH_4^+ adduct ions with the Orbitrap mass spectrometer to measure the oxygenated species for the first time. NH_4^+-Orbitrap is a promising CIMS technique for a comprehensive measurement of the whole product distribution and provides a more complete understanding of the molecular composition and volatility of OOMs. This allows NH_4^+-Orbitrap to better monitor the evolution of organic compounds, which can be beneficial for air quality, pollutant transport, and climate models. It is worth expecting that NH_4^+-Orbitrap can be not only useful for laboratory-based studies but also to field observations, to provide a deeper understanding of atmospheric oxidation processes. However, it remains challenging to accuratly quantify the concentrations of OOMs due to the absent signals of reagent ions. In addition, RH influences NH_4^+-Orbitrap sensitivity, which can be different for each OOM. Therefore, this specific effect requires more attention and dedicated studies before that the NH_4^+-Orbitrap can be used in field studies, for example, injection of pure or mixture of standards in atmospheric chamber at varying RH. From what is presented here, the understanding of RH effect on the NH_4^+-Orbitrap capabilities is too scarce to be able to understand the time series evolution of OOMs that would be obtained in the real atmosphere.

Conflicts of interest

There are no conflicts to declare.

Acknowledgements

We thank the European Organization for Nuclear Research (CERN) for supporting CLOUD with important technical and financial resources. We thank the Orbitool team for developing the tools to analyze mass spectra. This work was financially supported by the French National program LEFE (Les Enveloppes Fluides et l’Environnement), the European Research Council (ERC-StG MAARvEL; no. 852161), the European Union's Horizon 2020 research and innovation programme (Marie Sklodowska-Curie grant agreement no. 764991 and 701647), the Swiss National Science Foundation (no. 200021_169090, 200020_172602, 20FI20_172622, and 206021_198140), the US National Science Foundation (NSF_AGS_1801280, NSF_AGC_1801574, NSF_AGS_1801897, NSF_AGS_2132089), and the German Federal Ministry of Education and Research (CLOUD-16 01LK1601A). D.D.L. thanks the China Scholarship Council of P. R. China for the Ph.D. grant. M.Y.W. acknowledges financial support from the Schmidt Science Fellows Program by Schmidt Futures, in partnership with the Rhodes Trust.

Author Contributions

D.D.L., D.Y.W., L.C., W.S., M.Y.W., S.T., G.M., M.S., E.E., X.D.G., L.G.-C., M.G., J.P., B.R., B.S., P.R., S.P., A.H., J.C., J.K., N.M.D., C.G., I.E.-H., and M.R. prepared the CLOUD facility or measuring instruments. D.D.L., D.Y.W., L.C., W.S., M.Y.W., S.T., G.M., M.S., E.E., X.D.G., L.G.-C., M.G., J.P., B.R., B.S., J.K., and M.R. collected the CLOUD data. D.D.L., D.Y.W., L.C., W.S., M.Y.W., G.M., and M.R.and analysed the data. D.D.L., D.Y.W., M.Y.W., N.M.D., C.G., I.E.-H., and M.R. wrote the manuscript and contributed to the scientific discussion. All authors discussed the results and commented on the paper.

References

Berndt, T., Mentler, B., Scholz, W., Fischer, L., Herrmann, H., Kulmala, M., and Hansel, A.: Accretion Product Formation from Ozonolysis and OH Radical Reaction of α-Pinene: Mechanistic Insight and the Influence of Isoprene and Ethylene, Environmental Science & Technology, 52, 11069-11077, 10.1021/acs.est.8b02210, 2018a.

Berndt, T., Scholz, W., Mentler, B., Fischer, L., Herrmann, H., Kulmala, M., and Hansel, A.: Accretion Product Formation from Self- and Cross-Reactions of RO_2 Radicals in the Atmosphere, Angewandte Chemie International Edition, 57, 3820-3824, 10.1002/anie.201710989, 2018b.

Bianchi, F., Kurtén, T., Riva, M., Mohr, C., Rissanen, M. P., Roldin, P., Berndt, T., Crounse, J. D., Wennberg, P. O., Mentel, T. F., Wildt, J., Junninen, H., Jokinen, T., Kulmala, M., Worsnop, D. R., Thornton, J. A., Donahue, N., Kjaergaard, H. G., and Ehn, M.: Highly Oxygenated Organic Molecules (HOM) from Gas-Phase Autoxidation Involving Peroxy Radicals: A Key Contributor to Atmospheric Aerosol, Chemical Reviews, 119, 3472-3509, 10.1021/acs.chemrev.8b00395, 2019.

Bianchi, F., Tröstl, J., Junninen, H., Frege, C., Henne, S., Hoyle, C. R., Molteni, U., Herrmann, E., Adamov, A., Bukowiecki, N., Chen, X., Duplissy, J., Gysel, M., Hutterli, M., Kangasluoma, J., Kontkanen, J., Kürten, A., Manninen, H. E., Münch, S., Peräkylä, O., Petäjä, T., Rondo, L., Williamson, C., Weingartner, E., Curtius, J., Worsnop, D. R., Kulmala, M., Dommen, J., and Baltensperger, U.: New particle formation in the free troposphere: A question of chemistry and timing, Science, 352, 1109-1112, 10.1126/science.aad5456, 2016.

Breitenlechner, M., Fischer, L., Hainer, M., Heinritzi, M., Curtius, J., and Hansel, A.: PTR3: An Instrument for Studying the Lifecycle of Reactive Organic Carbon in the Atmosphere, Analytical Chemistry, 89, 5824-5831, 10.1021/acs.analchem.6b05110, 2017.

Cai, R., Huang, W., Meder, M., Bourgain, F., Aizikov, K., Riva, M., Bianchi, F., and Ehn, M.: Improving the Sensitivity of Fourier Transform Mass Spectrometer (Orbitrap) for Online Measurements of Atmospheric Vapors, Analytical Chemistry, 94, 15746-15753, 10.1021/acs.analchem.2c03403, 2022.

Cai, R., Li, Y., Clément, Y., Li, D., Dubois, C., Fabre, M., Besson, L., Perrier, S., George, C., Ehn, M., Huang, C., Yi, P., Ma, Y., and Riva, M.: Orbitool: a software tool for analyzing online Orbitrap mass spectrometry data, Atmospheric Measurement Techniques, 14, 2377-2387, 10.5194/amt-14-2377-2021, 2021.

Canaval, E., Hyttinen, N., Schmidbauer, B., Fischer, L., and Hansel, A.: NH_4^+ Association and Proton Transfer Reactions With a Series of Organic Molecules, Frontiers in Chemistry, 7, 10.3389/fchem.2019.00191, 2019.

Caudillo, L., Rörup, B., Heinritzi, M., Marie, G., Simon, M., Wagner, A. C., Müller, T., Granzin, M., Amorim, A., Ataei, F., Baalbaki, R., Bertozzi, B., Brasseur, Z., Chiu, R., Chu, B., Dada, L., Duplissy, J., Finkenzeller, H., Gonzalez Carracedo, L., He, X. C., Hofbauer, V., Kong, W., Lamkaddam, H., Lee, C. P., Lopez, B., Mahfouz, N. G. A., Makhmutov, V., Manninen, H. E., Marten, R., Massabò, D., Mauldin, R. L., Mentler, B., Molteni, U., Onnela, A., Pfeifer, J., Philippov, M., Piedehierro, A. A., Schervish, M., Scholz, W., Schulze, B., Shen, J., Stolzenburg, D., Stozhkov, Y., Surdu, M., Tauber, C., Tham, Y. J., Tian, P., Tomé, A., Vogt, S., Wang, M., Wang, D. S., Weber, S. K., Welti, A., Yonghong, W., Yusheng, W., Zauner-Wieczorek, M., Baltensperger, U., El Haddad, I., Flagan, R. C., Hansel, A., Höhler, K., Kirkby, J., Kulmala, M., Lehtipalo, K., Möhler, O., Saathoff, H., Volkamer, R., Winkler, P. M., Donahue, N. M., Kürten, A., and Curtius, J.: Chemical composition of nanoparticles from α-pinene nucleation and the influence of isoprene and relative humidity at low temperature, Atmospheric Chemistry and Physics, 21, 17099-17114, 10.5194/acp-21-17099-2021, 2021.

Daumit, K. E., Kessler, S. H., and Kroll, J. H.: Average chemical properties and potential formation pathways of highly oxidized organic aerosol, Faraday discussions, 165, 181-202, 10.1039/c3fd00045a, 2013.

Donahue, N. M., Epstein, S. A., Pandis, S. N., and Robinson, A. L.: A two-dimensional volatility basis set: 1. organic-aerosol mixing thermodynamics, Atmospheric Chemistry and Physics, 11, 3303-3318, 10.5194/acp-11-3303-2011, 2011.

Ehn, M., Junninen, H., Petäjä, T., Kurtén, T., Kerminen, V. M., Schobesberger, S., Manninen, H. E., Ortega, I. K., Vehkamäki, H., Kulmala, M., and Worsnop, D. R.: Composition and temporal behavior of ambient ions in the boreal forest, Atmospheric Chemistry and Physics, 10, 8513-8530, 10.5194/acp-10-8513-2010, 2010.

Ehn, M., Thornton, J. A., Kleist, E., Sipila, M., Junninen, H., Pullinen, I., Springer, M., Rubach, F., Tillmann, R., Lee, B., Lopez-Hilfiker, F., Andres, S., Acir, I. H., Rissanen, M., Jokinen, T., Schobesberger, S., Kangasluoma, J., Kontkanen, J., Nieminen, T., Kurten, T., Nielsen, L. B., Jorgensen, S., Kjaergaard, H. G., Canagaratna, M., Maso, M. D., Berndt, T., Petaja, T., Wahner, A., Kerminen, V. M., Kulmala, M., Worsnop, D. R., Wildt, J., and Mentel, T. F.: A large source of low-volatility secondary organic aerosol, Nature, 506, 476-479, 10.1038/nature13032, 2014.

Fan, J., Wang, Y., Rosenfeld, D., and Liu, X.: Review of Aerosol–Cloud Interactions: Mechanisms, Significance, and Challenges, Journal of the Atmospheric Sciences, 73, 4221-4252, 10.1175/jas-d-16-0037.1, 2016.

Hallquist, M., Wenger, J. C., Baltensperger, U., Rudich, Y., Simpson, D., Claeys, M., Dommen, J., Donahue, N. M., George, C., Goldstein, A. H., Hamilton, J. F., Herrmann, H., Hoffmann, T., Iinuma, Y., Jang, M., Jenkin, M. E., Jimenez, J. L., Kiendler-Scharr, A., Maenhaut, W., McFiggans, G., Mentel, T. F., Monod, A., Prévôt, A. S. H., Seinfeld, J. H., Surratt, J. D., Szmigielski, R., and Wildt, J.: The formation, properties and impact of secondary organic aerosol: current and emerging issues, Atmospheric Chemistry and Physics, 9, 5155-5236, 10.5194/acp-9-5155-2009, 2009.

Hansel, A., Scholz, W., Mentler, B., Fischer, L., and Berndt, T.: Detection of RO_2 radicals and other products from cyclohexene ozonolysis with NH_4^+ and acetate chemical ionization mass spectrometry, Atmospheric Environment, 186, 248-255, 10.1016/j.atmosenv.2018.04.023, 2018.

Haywood, J. and Boucher, O.: Estimates of the direct and indirect radiative forcing due to tropospheric aerosols: A review, Reviews of Geophysics, 38, 513-543, 10.1029/1999rg000078, 2000.

Heinritzi, M., Simon, M., Steiner, G., Wagner, A. C., Kürten, A., Hansel, A., and Curtius, J.: Characterization of the mass-dependent transmission efficiency of a CIMS, Atmospheric Measurement Techniques, 9, 1449-1460, 10.5194/amt-9-1449-2016, 2016.

Huang, W., Li, H., Sarnela, N., Heikkinen, L., Tham, Y. J., Mikkilä, J., Thomas, S. J., Donahue, N. M., Kulmala, M., and Bianchi, F.: Measurement report: Molecular composition and volatility of gaseous organic compounds in a boreal forest – from volatile organic compounds to highly oxygenated organic molecules, Atmospheric Chemistry and Physics, 21, 8961-8977, 10.5194/acp-21-8961-2021, 2021.

Isaacman-VanWertz, G. and Aumont, B.: Impact of organic molecular structure on the estimation of atmospherically relevant physicochemical parameters, Atmospheric Chemistry and Physics, 21, 6541-6563, 10.5194/acp-21-6541-2021, 2021.

Jimenez, J. L., Canagaratna, M. R., Donahue, N. M., Prevot, A. S. H., Zhang, Q., Kroll, J. H., DeCarlo, P. F., Allan, J. D., Coe, H., Ng, N. L., Aiken, A. C., Docherty, K. S., Ulbrich, I. M., Grieshop, A. P., Robinson, A. L., Duplissy, J., Smith, J. D., Wilson, K. R., Lanz, V. A., Hueglin, C., Sun, Y. L., Tian, J., Laaksonen, A., Raatikainen, T., Rautiainen, J., Vaattovaara, P., Ehn, M., Kulmala, M., Tomlinson, J. M., Collins, D. R., Cubison, M. J., Dunlea, J., Huffman, J. A., Onasch, T. B., Alfarra, M. R., Williams, P. I., Bower, K., Kondo, Y., Schneider, J., Drewnick, F., Borrmann, S., Weimer, S., Demerjian, K., Salcedo, D., Cottrell, L., Griffin, R., Takami, A., Miyoshi, T., Hatakeyama, S., Shimono, A., Sun, J. Y., Zhang, Y. M., Dzepina, K., Kimmel, J. R., Sueper, D., Jayne, J. T., Herndon, S. C., Trimborn, A. M., Williams, L. R., Wood, E. C., Middlebrook, A. M., Kolb, C. E., Baltensperger, U., and Worsnop, D. R.: Evolution of Organic Aerosols in the Atmosphere, Science, 326, 1525-1529, doi:10.1126/science.1180353, 2009.

Jokinen, T., Sipilä, M., Junninen, H., Ehn, M., Lönn, G., Hakala, J., Petäjä, T., Mauldin, R. L., Kulmala, M., and Worsnop, D. R.: Atmospheric sulphuric acid and neutral cluster measurements using CI-APi-TOF, Atmospheric Chemistry and Physics, 12, 4117-4125, 10.5194/acp-12-4117-2012, 2012.

Kirkby, J., Duplissy, J., Sengupta, K., Frege, C., Gordon, H., Williamson, C., Heinritzi, M., Simon, M., Yan, C., Almeida, J., Tröstl, J., Nieminen, T., Ortega, I. K., Wagner, R., Adamov, A., Amorim, A., Bernhammer, A.-K., Bianchi, F., Breitenlechner, M., Brilke, S., Chen, X., Craven, J., Dias, A., Ehrhart, S., Flagan, R. C., Franchin, A., Fuchs, C., Guida, R., Hakala, J., Hoyle, C. R., Jokinen, T., Junninen, H., Kangasluoma, J., Kim, J., Krapf, M., Kürten, A., Laaksonen, A., Lehtipalo, K., Makhmutov, V., Mathot, S., Molteni, U., Onnela, A., Peräkylä, O., Piel, F., Petäjä, T., Praplan, A. P., Pringle, K., Rap, A., Richards, N. A. D., Riipinen, I., Rissanen, M. P., Rondo, L., Sarnela, N., Schobesberger, S., Scott, C. E., Seinfeld, J. H., Sipilä, M., Steiner, G., Stozhkov, Y., Stratmann, F., Tomé, A., Virtanen, A., Vogel, A. L., Wagner, A. C., Wagner, P. E., Weingartner, E., Wimmer, D., Winkler, P. M., Ye, P., Zhang, X., Hansel, A., Dommen, J., Donahue, N. M., Worsnop, D. R., Baltensperger, U., Kulmala, M., Carslaw, K. S., and Curtius, J.: Ion-induced nucleation of pure biogenic particles, Nature, 533, 521, 10.1038/nature17953, 2016.

Lee, B. H., Lopez-Hilfiker, F. D., Mohr, C., Kurtén, T., Worsnop, D. R., and Thornton, J. A.: An Iodide-Adduct High-Resolution Time-of-Flight Chemical-Ionization Mass Spectrometer: Application to Atmospheric Inorganic and Organic Compounds, Environmental Science & Technology, 48, 6309-6317, 10.1021/es500362a, 2014.

Li, Y., Pöschl, U., and Shiraiwa, M.: Molecular corridors and parameterizations of volatility in the chemical evolution of organic aerosols, Atmospheric Chemistry and Physics, 16, 3327-3344, 10.5194/acp-16-3327-2016, 2016.

Lopez-Hilfiker, F. D., Mohr, C., Ehn, M., Rubach, F., Kleist, E., Wildt, J., Mentel, T. F., Lutz, A., Hallquist, M., Worsnop, D., and Thornton, J. A.: A novel method for online analysis of gas and particle composition: description and evaluation of a Filter Inlet for Gases and AEROsols (FIGAERO), Atmospheric Measurement Techniques, 7, 983-1001, 10.5194/amt-7-983-2014, 2014.

Mellouki, A., Wallington, T. J., and Chen, J.: Atmospheric chemistry of oxygenated volatile organic compounds: impacts on air quality and climate, Chemical reviews, 115, 3984-4014, 10.1021/cr500549n, 2015.

Mohr, C., Thornton, J. A., Heitto, A., Lopez-Hilfiker, F. D., Lutz, A., Riipinen, I., Hong, J., Donahue, N. M., Hallquist, M., Petäjä, T., Kulmala, M., and Yli-Juuti, T.: Molecular identification of organic vapors driving atmospheric nanoparticle growth, Nature Communications, 10, 10.1038/s41467-019-12473-2, 2019.

Pospisilova, V., Lopez-Hilfiker, F. D., Bell, D. M., El Haddad, I., Mohr, C., Huang, W., Heikkinen, L., Xiao, M., Dommen, J., Prevot, A. S. H., Baltensperger, U., and Slowik, J. G.: On the fate of oxygenated organic molecules in atmospheric aerosol particles, Science Advances, 6, eaax8922, doi:10.1126/sciadv.aax8922, 2020.

Rissanen, M. P., Mikkilä, J., Iyer, S., and Hakala, J.: Multi-scheme chemical ionization inlet (MION) for fast switching of reagent ion chemistry in atmospheric pressure chemical ionization mass spectrometry (CIMS) applications, Atmospheric Measurement Techniques, 12, 6635-6646, 10.5194/amt-12-6635-2019, 2019.

Riva, M., Brüggemann, M., Li, D., Perrier, S., George, C., Herrmann, H., and Berndt, T.: Capability of CI-Orbitrap for Gas-Phase Analysis in Atmospheric Chemistry: A Comparison with the CI-APi-TOF Technique, Analytical Chemistry, 92, 8142-8150, 10.1021/acs.analchem.0c00111, 2020.

Riva, M., Ehn, M., Li, D., Tomaz, S., Bourgain, F., Perrier, S., and George, C.: CI-Orbitrap: An Analytical Instrument To Study Atmospheric Reactive Organic Species, Analytical Chemistry, 91, 9419-9423, 10.1021/acs.analchem.9b02093, 2019a.

Riva, M., Rantala, P., Krechmer, J. E., Peräkylä, O., Zhang, Y., Heikkinen, L., Garmash, O., Yan, C., Kulmala, M., Worsnop, D., and Ehn, M.: Evaluating the performance of five different chemical ionization techniques for detecting gaseous oxygenated organic species, Atmospheric Measurement Techniques, 12, 2403-2421, 10.5194/amt-12-2403-2019, 2019b.

Schobesberger, S., Junninen, H., Bianchi, F., Lonn, G., Ehn, M., Lehtipalo, K., Dommen, J., Ehrhart, S., Ortega, I. K., Franchin, A., Nieminen, T., Riccobono, F., Hutterli, M., Duplissy, J., Almeida, J., Amorim, A., Breitenlechner, M., Downard, A. J., Dunne, E. M., Flagan, R. C., Kajos, M., Keskinen, H., Kirkby, J., Kupc, A., Kurten, A., Kurten, T., Laaksonen, A., Mathot, S., Onnela, A., Praplan, A. P., Rondo, L., Santos, F. D., Schallhart, S., Schnitzhofer, R., Sipila, M., Tome, A., Tsagkogeorgas, G., Vehkamaki, H., Wimmer, D., Baltensperger, U., Carslaw, K. S., Curtius, J., Hansel, A., Petaja, T., Kulmala, M., Donahue, N. M., and Worsnop, D. R.: Molecular understanding of atmospheric particle formation from sulfuric acid and large oxidized organic molecules, Proceedings of the National Academy of Sciences of the United States of America, 110, 17223-17228, 10.1073/pnas.1306973110, 2013.

Simon, M., Dada, L., Heinritzi, M., Scholz, W., Stolzenburg, D., Fischer, L., Wagner, A. C., Kürten, A., Rörup, B., He, X.-C., Almeida, J., Baalbaki, R., Baccarini, A., Bauer, P. S., Beck, L., Bergen, A., Bianchi, F., Bräkling, S., Brilke, S., Caudillo, L., Chen, D., Chu, B., Dias, A., Draper, D. C., Duplissy, J., El-Haddad, I., Finkenzeller, H., Frege, C., Gonzalez-Carracedo, L., Gordon, H., Granzin, M., Hakala, J., Hofbauer, V., Hoyle, C. R., Kim, C., Kong, W., Lamkaddam, H., Lee, C. P., Lehtipalo, K., Leiminger, M., Mai, H., Manninen, H. E., Marie, G., Marten, R., Mentler, B., Molteni, U., Nichman, L., Nie, W., Ojdanic, A., Onnela, A., Partoll, E., Petäjä, T., Pfeifer, J., Philippov, M., Quéléver, L. L. J., Ranjithkumar, A., Rissanen, M. P., Schallhart, S., Schobesberger, S., Schuchmann, S., Shen, J., Sipilä, M., Steiner, G., Stozhkov, Y., Tauber, C., Tham, Y. J., Tomé, A. R., Vazquez-Pufleau, M., Vogel, A. L., Wagner, R., Wang, M., Wang, D. S., Wang, Y., Weber, S. K., Wu, Y., Xiao, M., Yan, C., Ye, P., Ye, Q., Zauner-Wieczorek, M., Zhou, X., Baltensperger, U., Dommen, J., Flagan, R. C., Hansel, A., Kulmala, M., Volkamer, R., Winkler, P. M., Worsnop, D. R., Donahue, N. M., Kirkby, J., and Curtius, J.: Molecular understanding of new-particle formation from α-pinene between −50 and +25 °C, Atmospheric Chemistry and Physics, 20, 9183-9207, 10.5194/acp-20-9183-2020, 2020.

Stolzenburg, D., Fischer, L., Vogel, A. L., Heinritzi, M., Schervish, M., Simon, M., Wagner, A. C., Dada, L., Ahonen, L. R., Amorim, A., Baccarini, A., Bauer, P. S., Baumgartner, B., Bergen, A., Bianchi, F., Breitenlechner, M., Brilke, S., Buenrostro Mazon, S., Chen, D., Dias, A., Draper, D. C., Duplissy, J., El Haddad, I., Finkenzeller, H., Frege, C., Fuchs, C., Garmash, O., Gordon, H., He, X., Helm, J., Hofbauer, V., Hoyle, C. R., Kim, C., Kirkby, J., Kontkanen, J., Kürten, A., Lampilahti, J., Lawler, M., Lehtipalo, K., Leiminger, M., Mai, H., Mathot, S., Mentler, B., Molteni, U., Nie, W., Nieminen, T., Nowak, J. B., Ojdanic, A., Onnela, A., Passananti, M., Petäjä, T., Quéléver, L. L. J., Rissanen, M. P., Sarnela, N., Schallhart, S., Tauber, C., Tomé, A., Wagner, R., Wang, M., Weitz, L., Wimmer, D., Xiao, M., Yan, C., Ye, P., Zha, Q., Baltensperger, U., Curtius, J., Dommen, J., Flagan, R. C., Kulmala, M., Smith, J. N., Worsnop, D. R., Hansel, A., Donahue, N. M., and Winkler, P. M.: Rapid growth of organic aerosol nanoparticles over a wide tropospheric temperature range, Proceedings of the National Academy of Sciences, 115, 9122-9127, 10.1073/pnas.1807604115, 2018.

Surdu, M., Lamkaddam, H., Wang, D. S., Bell, D. M., Xiao, M., Lee, C. P., Li, D., Caudillo, L., Marie, G., Scholz, W., Wang, M., Lopez, B., Piedehierro, A. A., Ataei, F., Baalbaki, R., Bertozzi, B., Bogert, P., Brasseur, Z., Dada, L., Duplissy, J., Finkenzeller, H., He, X.-C., Höhler, K., Korhonen, K., Krechmer, J. E., Lehtipalo, K., Mahfouz, N. G. A., Manninen, H. E., Marten, R., Massabò, D., Mauldin, R., Petäjä, T., Pfeifer, J., Philippov, M., Rörup, B., Simon, M., Shen, J., Umo, N. S., Vogel, F., Weber, S. K., Zauner-Wieczorek, M., Volkamer, R., Saathoff, H., Möhler, O., Kirkby, J., Worsnop, D. R., Kulmala, M., Stratmann, F., Hansel, A., Curtius, J., Welti, A., Riva, M., Donahue, N. M., Baltensperger, U., and El Haddad, I.: Molecular Understanding of the Enhancement in Organic Aerosol Mass at High Relative Humidity, Environmental Science & Technology, 57, 2297-2309, 10.1021/acs.est.2c04587, 2023.

Viggiano, A. A., Seeley, J. V., Mundis, P. L., Williamson, J. S., and Morris, R. A.: Rate Constants for the Reactions of $XO_3^-(H_2O)_n$ (X = C, HC, and N) and $NO_3^-(HNO_3)n$ with H_2SO_4: Implications for Atmospheric Detection of H_2SO_4, The Journal of Physical Chemistry A, 101, 8275-8278, 10.1021/jp971768h, 1997.

Wang, M., Kong, W., Marten, R., He, X.-C., Chen, D., Pfeifer, J., Heitto, A., Kontkanen, J., Dada, L., Kürten, A., Yli-Juuti, T., Manninen, H. E., Amanatidis, S., Amorim, A., Baalbaki, R., Baccarini, A., Bell, D. M., Bertozzi, B., Bräkling, S., Brilke, S., Murillo, L. C., Chiu, R., Chu, B., De Menezes, L.-P., Duplissy, J., Finkenzeller, H., Carracedo, L. G., Granzin, M., Guida, R., Hansel, A., Hofbauer, V., Krechmer, J., Lehtipalo, K., Lamkaddam, H., Lampimäki, M., Lee, C. P., Makhmutov, V., Marie, G., Mathot, S., Mauldin, R. L., Mentler, B., Müller, T., Onnela, A., Partoll, E., Petäjä, T., Philippov, M., Pospisilova, V., Ranjithkumar, A., Rissanen, M., Rörup, B., Scholz, W., Shen, J., Simon, M., Sipilä, M., Steiner, G., Stolzenburg, D., Tham, Y. J., Tomé, A., Wagner, A. C., Wang, D. S., Wang, Y., Weber, S. K., Winkler, P. M., Wlasits, P. J., Wu, Y., Xiao, M., Ye, Q., Zauner-Wieczorek, M., Zhou, X., Volkamer, R., Riipinen, I., Dommen, J., Curtius, J., Baltensperger, U., Kulmala, M., Worsnop, D. R., Kirkby, J., Seinfeld, J. H., El-Haddad, I., Flagan, R. C., and Donahue, N. M.: Rapid growth of new atmospheric particles by nitric acid and ammonia condensation, Nature, 581, 184-189, 10.1038/s41586-020-2270-4, 2020.

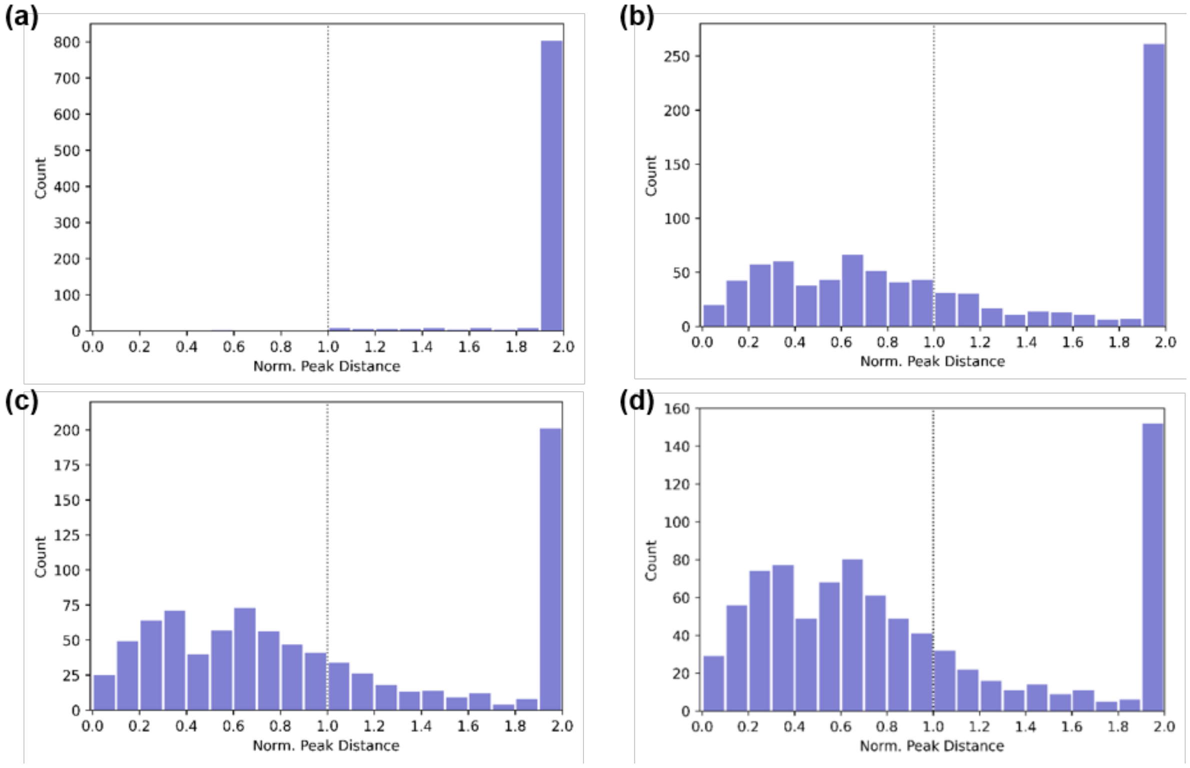

Figure 1: Number of adjacent peaks within a intensity threshold as the function of normalized peak distance observed by (a) NH_4^+-Orbitrap and (b, c, d) NH_4^+-TOF, respectively. The normalized peak distance was the ratio of distance between neighboring peaks to the full width at half maximum (FWHM). For each ion, the distance to the closest neighbor with a relative peak intensity that exceeded 20%, 50%, or 100% is recorded. (a) Orbitrap mass analyzer >99% of ions were separated by at least 1 FWHM from their neighbors with relative intensity threshold being set at 20%. (b) TOF mass analyzer (mass resolution ~10,000) >46% of ions were separated by at least 1 FWHM from their neighbors with a relative intensity threshold being set at 100%. (c) TOF mass analyzer >39% of ions were separated by at least 1 FWHM from their neighbors with a relative intensity threshold being set at 50%. (d) TOF mass analyzer >32% of ions were separated by at least 1 FWHM from their neighbors with a relative intensity threshold being set at 20%.

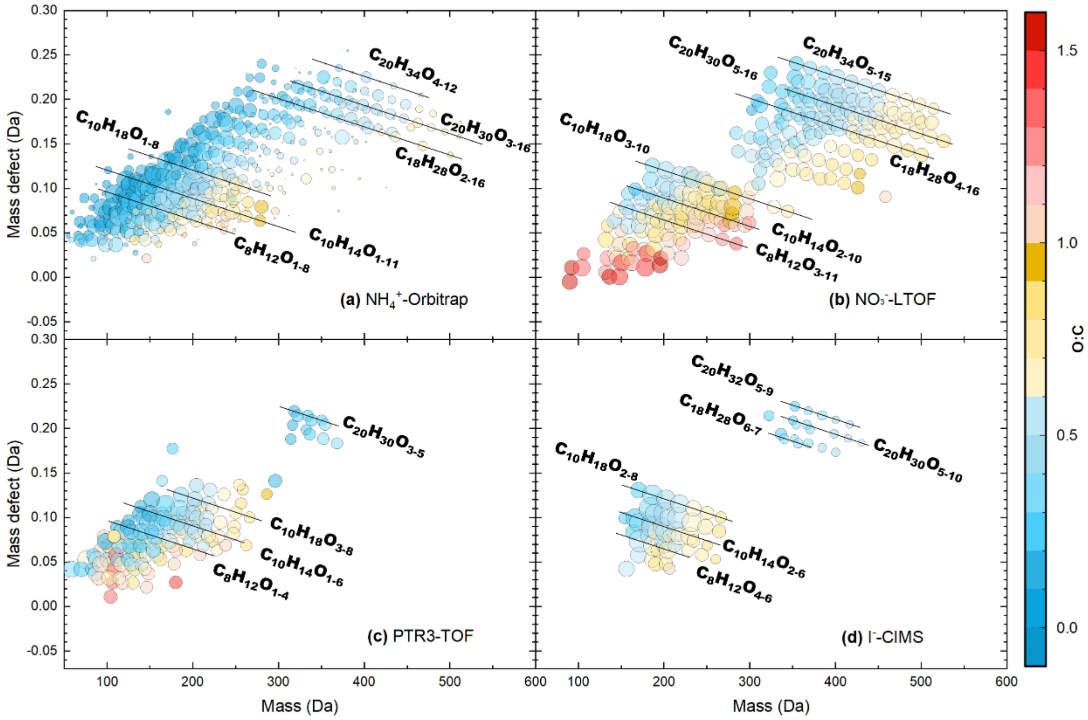

Figure 2: Mass defect plots for organic compounds measured by (a) NH_4^+-Orbitrap, (b) NO_3^--LTOF, (c) PTR3-TOF and (d) I^--CIMS in run 2211. The x-axis represents the mass-to-charge ratio of the neutral analyte and the y-axis represents the corresponding mass defect, which is the difference between their exact mass and nominal mass (Schobesberger et al., 2013). Markers were all sized by the logarithm of their corresponding signals and colored by the O:C value. Some major OOMs measured by different instruments were indicated by the black lines.

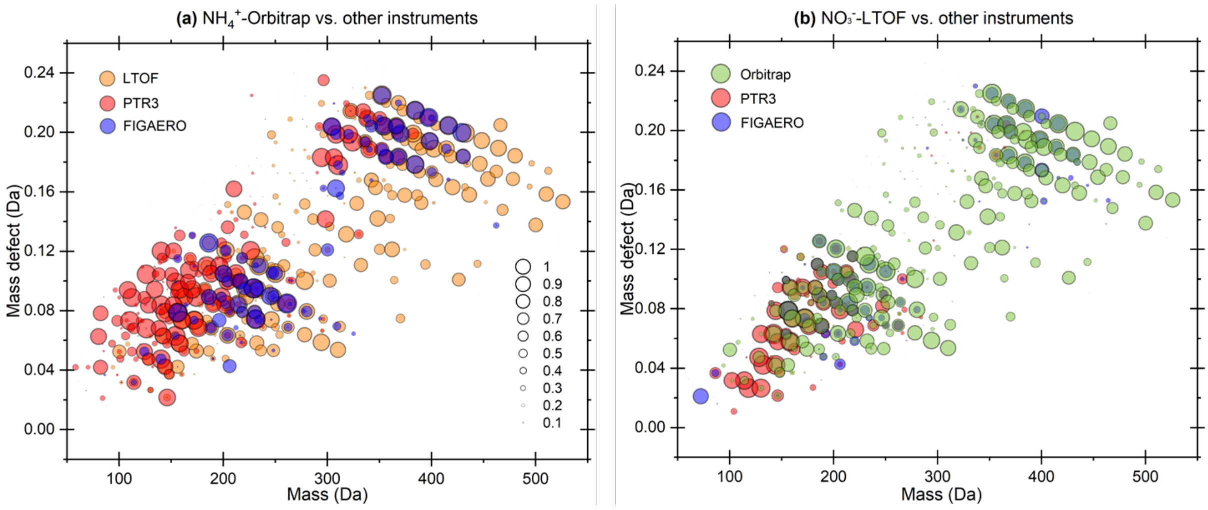

Figure 3: Mass defect plots depicting the compounds of which time series correlation was observed by (a) NH_4^+-Orbitrap and (b) NO_3^--LTOF with other MS instruments. Each circle represents a molecule and marker size represents the correlation R^2 of time series of the molecules between two different MS instruments. Two sets of data in run 2211 and 2213 were used to reduce uncertainties.

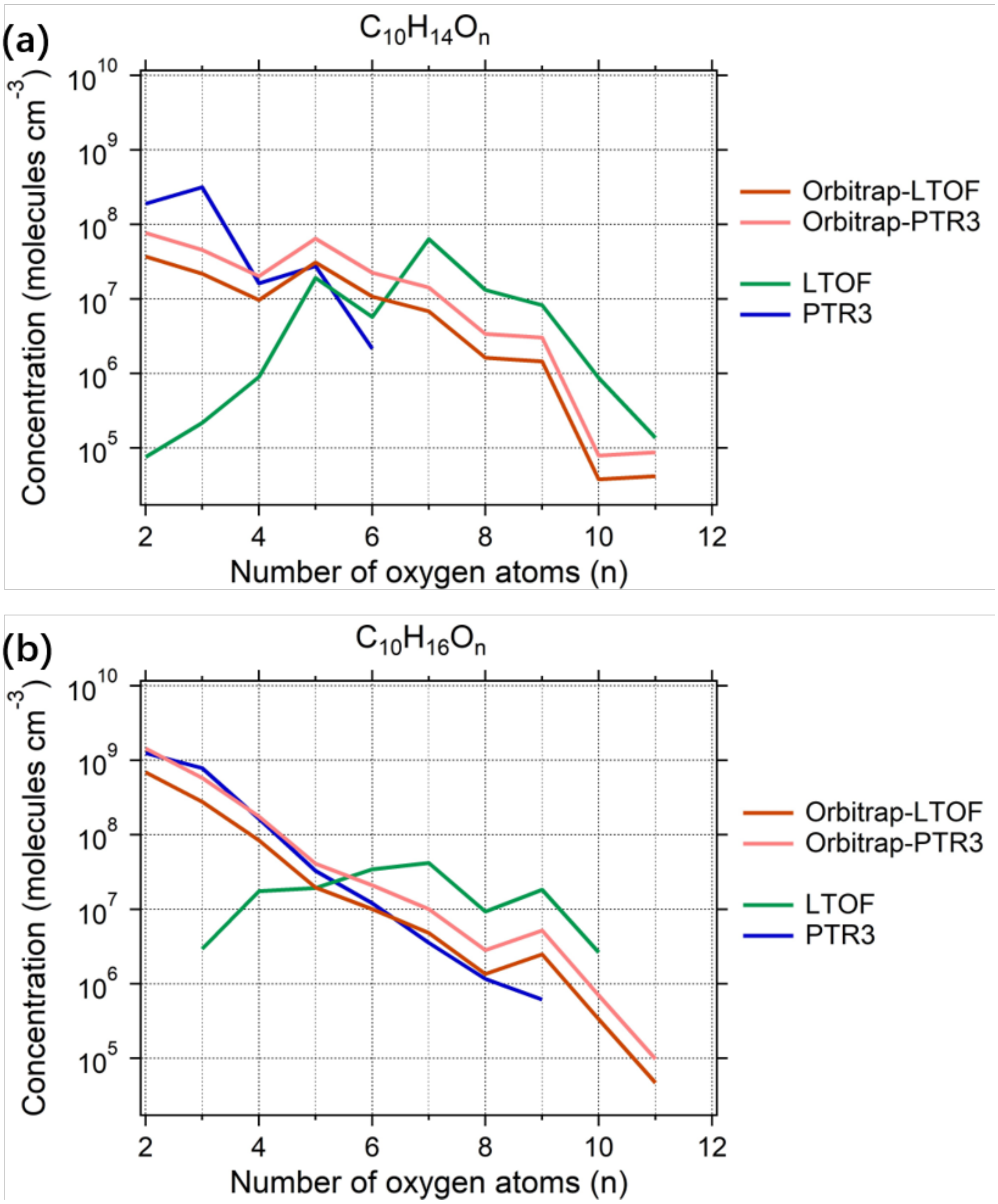

Figure 4: Estimated concentrations of the main C_{10} oxidation products (a) $C_{10}H_{14}O_n$ and (b) $C_{10}H_{16}O_n$ as a function of oxygen numbers observed in run 2211. Orbitrap-LTOF and Orbitrap-PTR3 represented the estimated concentration of monomers measured by NH_4^+-Orbitrap using the calibration factors from the correlation analysis with NO_3^--LTOF and PTR3-TOF, respectively.

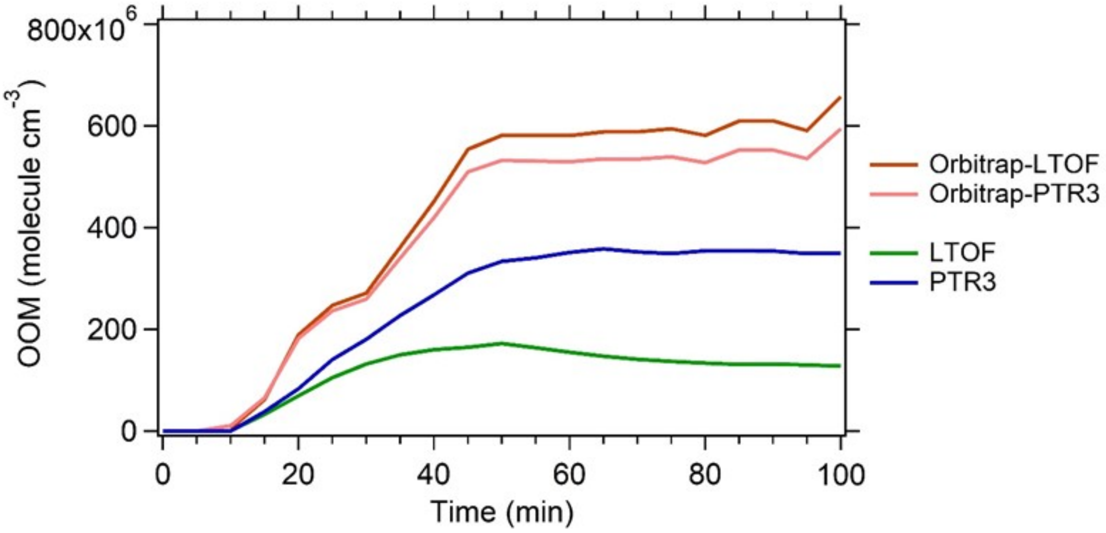

Figure 5: Estimated concentrations of all measured OOMs in the photooxidation of α-pinene. All monomers C_{8-10} and dimers C_{18-20} measured by NH_4^+-Orbitrap, NO_3^--LTOF, and PTR3-TOF in run 2213 were summed up. The concentrations of OOMs measured by NH_4^+-Orbitrap were quantified by the calibration factors derived from correlation analysis between NH_4^+-Orbitrap and NO_3^--LTOF (Orbitrap-LTOF, light green) or PTR3-TOF (Orbitrap-PTR3, light blue), respectively.

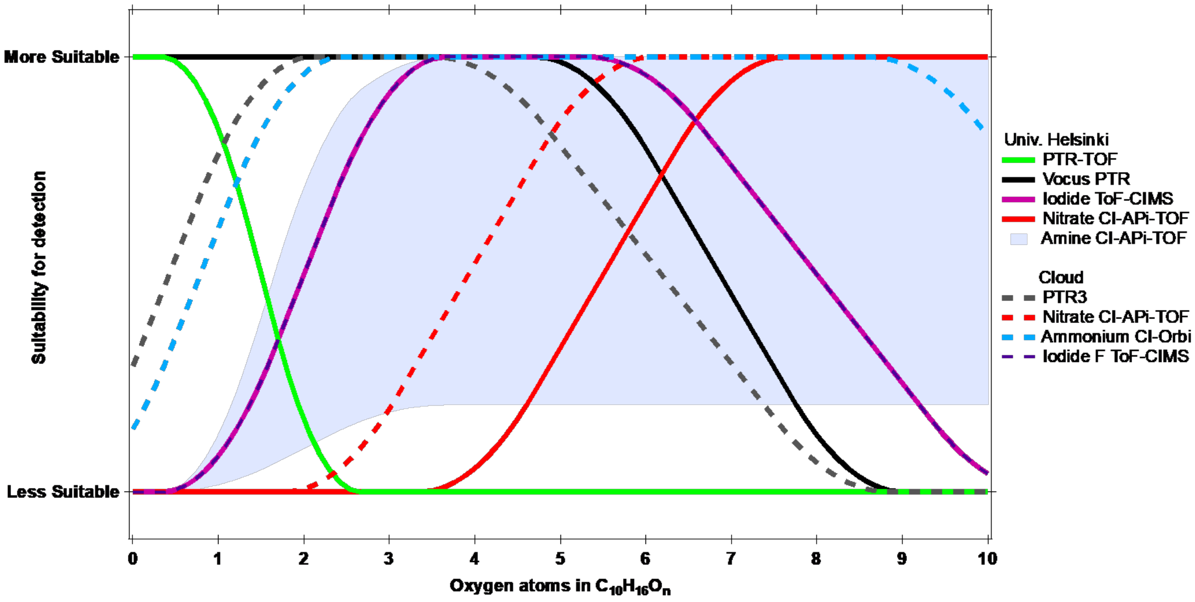

Figure 6: Estimated detection suitability of the different CIMS techniques for monomers from α-pinene ozonolysis, plotted as a function of the number of oxygen atoms. Image modified from Riva et al.(Riva et al., 2019b).

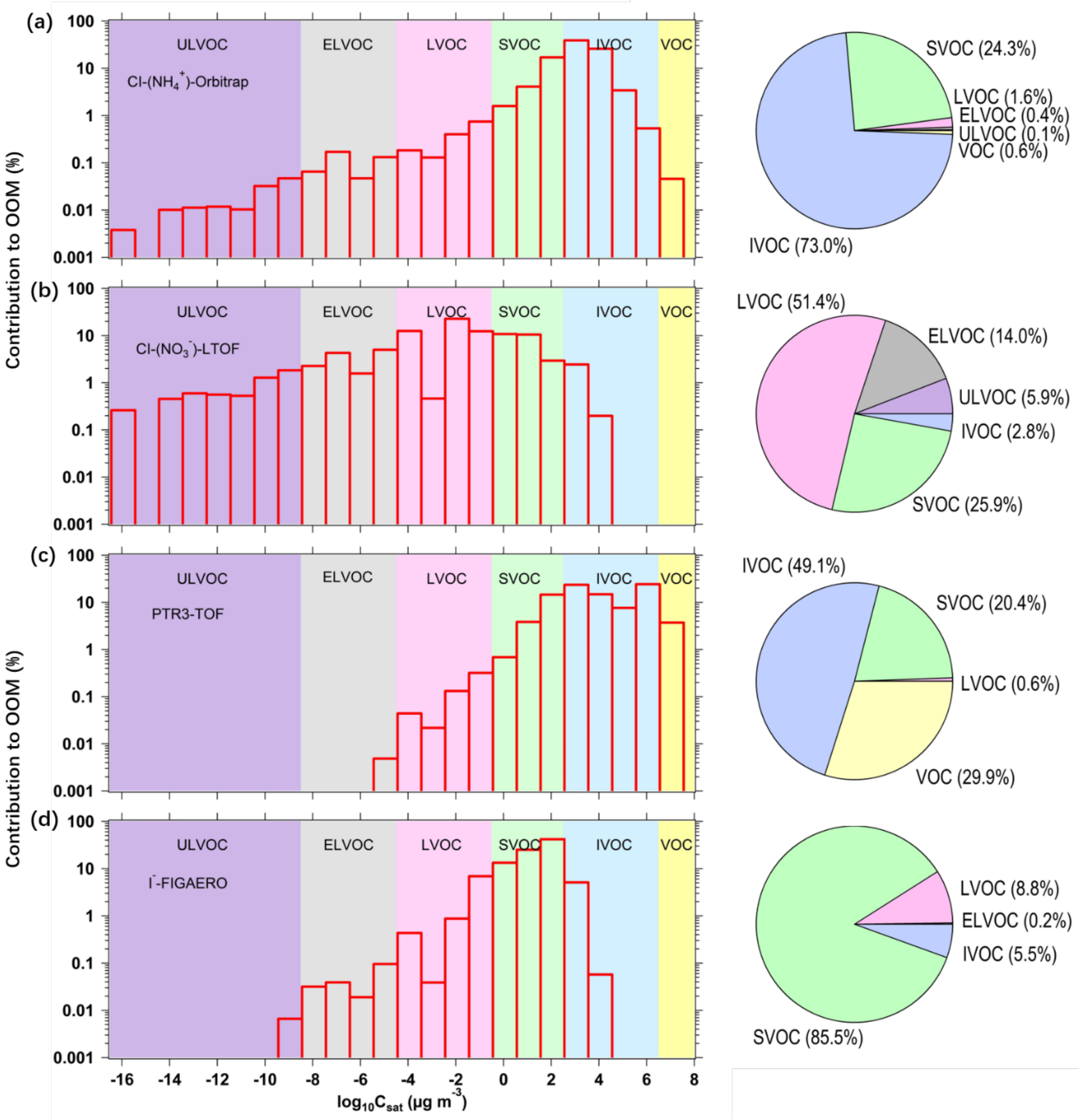

Figure 7: Volatility distribution comparison for organic compounds detected by (a) NH_4^+-Orbitrap, (b) NO_3^--LTOF, (c) PTR3-TOF and (d) I^--CIMS. The background colors represent the saturation concentration (C_{sat}) in the range of ultra-low volatility (ULVOCs, purple), extremely low volatility (ELVOCs, gray), low volatility (LVOCs, pink), semi-volatile (SVOCs, green), intermediate volatility (IVOCs, blue) and volatile organic compounds (VOCs). The right pie charts are the corresponding contributions of VOC, IVOC, SVOC, LVOC, ELVOC, and ULVOC classes in run 2211. Concentrations were used to calculate the contribution in each volatility bin for NO_3^--LTOF and PTR3-TOF, while signals were calculated for NH_4^+-Orbitrap and I^--CIMS.

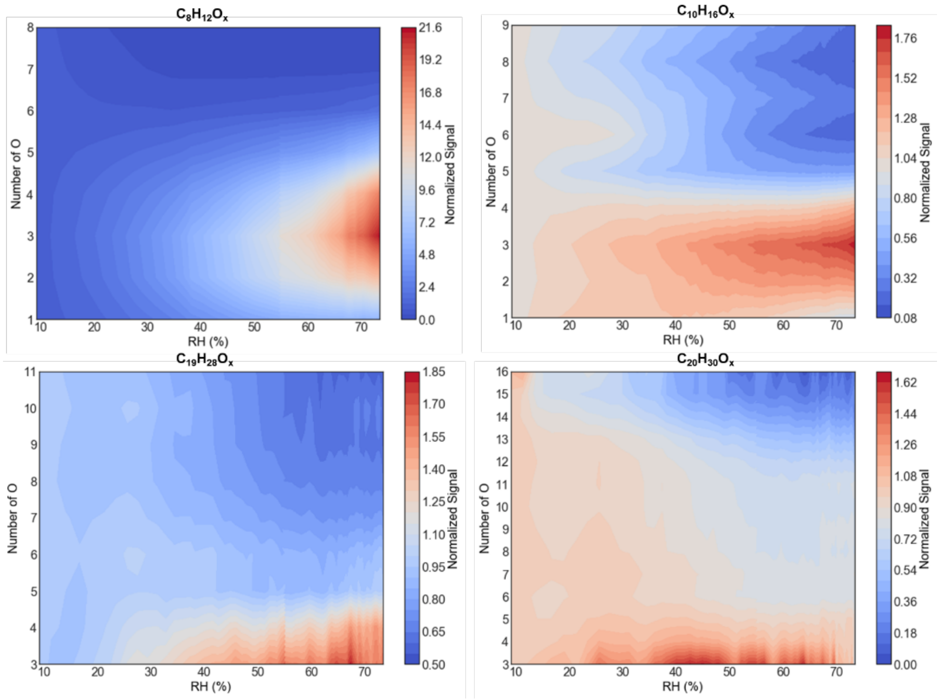

Figure 8: The effect of relative humidity on the distribution of the most abundant monomers and dimers measured by NH_4^+-Orbitrap. The RH ramped from ~10% to ~80% in run 2211. The normalized signal represents the signal variation ratio at certain RH compared to that at RH = 10%, normalized signal = $\frac{signal_{RH}}{signal_{10\%}}$.